*Bull. Nov. Comp. Center*, Num. Anal., 16 (2013), 23–42


# GPUPEGAS: a new GPU-accelerated hydrodynamic code for numerical simulation of interacting galaxies*

Igor Kulikov

**Abstract.** In this paper, a new scalable hydrodynamic code GPUPEGAS (GPU-accelerated Performance Gas Astrophysical Simulation) for the simulation of interacting galaxies is proposed. This code is based on a combination of the Godunov method as well as on the original implementation of the FlIC method, specially adapted to the GPU-implementation. Fast Fourier Transform is used for the Poisson equation solution in GPUPEGAS. Software implementation of the above methods was tested on classical gas dynamics problems, new Aksenov's test and classical gravitational gas dynamics problems. Collisionless hydrodynamic approach was used for modeling of stars and dark matter. The scalability of GPUPEGAS computational accelerators is shown.

## 1. Introduction

The movement of galaxies in dense clusters turns the collisions of galaxies into an important evolutionary factor [1, 2]. Numerical simulation plays the key role in studying these processes. Due to an extremely high growth of supercomputer performance, the new astrophysical models and codes need to be developed for a detailed simulation of different physical effects in astrophysics.

During the last 15 years, from a wide range of the hydrodynamic methods, two main approaches are used for non-stationary astrophysical problems solution. They are the Lagrangian SPH method [3, 4] (Smoothed Particle Hydrodynamics) and the Eulerian methods within adaptive meshes, or AMR [6] (Adaptive Mesh Refinement). During the last 5 years, a lot of combined codes (using both the Lagrangian and the Eulerian approaches) appeared.

The main problem of the SPH codes is the search for neighbors for a particle and the computation of gravitational interaction between particles.

*Supported by the Federal Programme "Scientific and Scientific-Pedagogical Cadres Innovation Russia for 2009–2013" and Federal Programme for the Development of Priority Areas of Russian Scientific and Technological Complex 2007–2013, the Russian Ministry of Education and Sciences, RFBR under Grant 12-01-31352 for Junior Researchers, and by the Grant of President of the Russian Federation for supporting young scientists, MK–4183.2013.9.

In order to solve these problems, many algorithms were developed: particle-particle/particle-mesh or $P^3M$ method [7], adaptation of $P^3M$ method using the hierarchy of computational meshes $AP^3M$ [8], the tree code [9], a combination of the tree code and the particle-mesh method, that is Tree-PM method [10]. There are certain methods used for solving the Poisson equation: the conjugate gradient method, the fast Fourier transform, the method of successive over-relaxation and the Fedorenko method (Multigrid method) [11].

For the numerical solution of gas dynamics problems, the Godunov method is widely used [12], thats main structural element is a Riemann problem. Different algorithms of the Riemann problem solution have produced a wide class of mathematical methods [13, 14]. The main methods are the Courant–Isakson–Reese method [15] and the Roe method [16]. These methods are based on linearized hyperbolic systems of equations [17], where the solution to the Riemann problem is constructed only from the Riemann waves. The main approach of wave velocity evaluation is a double wave Harten–Lax–Van Leer(HLL) scheme [18] and its modification — the HLLE-method [19], HLLC [20]. Some schemes, based on the Godunov method, such as upwind second order MUSCL [21] and the TVD schemes [26], the third order piecewise parabolic method (PPM) [5] were developed. Still it is not clear how to determine the order of accuracy of a scheme in the case of a discontinuous solution as is stated in [27].

The most well-known SPH codes are Hydra [22], Gasoline [23], Grape-SPH [24], GADGET [25]. The most well-known mesh codes (in some cases with adaptive mesh refinement) are NIRVANA [28], FLASH [29], ZEUS-MP [30], ENZO [6], RAMSES [31], ART [32], Athena [33], Pencil Code [34], Heracles [40], Orion [41], Pluto [42], CASTRO [43], GAMER [35]. BETHE-Hydro [36], AREPO [37], CHIMERA [38] and PEGAS [39] (designed by the author of the present paper) codes are based on the mixed Lagrangian and Eulerian approaches. A large number of existing astrophysical codes means that there is no perfect code suitable for all the cases. In such a way, new code development as well as a modification of existing codes is still necessary. In spite of the development of PETAFLOPs astrophysics codes such as PetaGADGET [44], Enzo-P, PetaART, it is necessary to note some scalability restrictions of both the AMR and the SPH methods [45, 46].

The present paper contains a description of a new collisionless component of galaxies on the basis of “Collisionless hydrodynamic” model. For the first time, the model for astrophysical problems was used in [47]. GPUPEGAS is the first code, which contains the full Boltzmann moment equations with a complete symmetric velocity dispersion tensor. The objective of this paper is a detailed description of the numerical method as well as of peculiarities of the implementation of the method for hydrid supercomputers equipped with GPU-accelerated hydrodynamic code.

## 2. Numerical method description

We will use a two-phase approach for modeling the interacting galaxies: a hydrodynamic component [39] and a collisionless component [47] for the description of the stars and dark matter.

We use for a hydrodynamic component a 3D model of self-gravitating gas dynamics in the Cartesian coordinate system:

$$\frac{\partial \rho}{\partial t} + \frac{\partial \rho v_k}{\partial x_k} = 0,$$
$$\frac{\partial \rho v_i}{\partial t} + \frac{\partial \rho v_i v_k}{\partial x_k} = -\frac{\partial p}{\partial x_i} - \rho \frac{\partial (\Phi + \Phi_0)}{\partial x_i},$$
$$\frac{\partial \rho E}{\partial t} + \frac{\partial \rho E v_k}{\partial x_k} = -\frac{\partial p v_k}{\partial x_k} - \rho v_k \frac{\partial (\Phi + \Phi_0)}{\partial x_k} - q,$$
$$\frac{\partial \rho \epsilon}{\partial t} + \frac{\partial \rho \epsilon v_k}{\partial x_k} = -(\gamma - 1)\rho\epsilon \frac{\partial v_k}{\partial x_k} - q,$$
$$\Delta\Phi = 4\pi\rho, \qquad p = (\gamma - 1)\rho\epsilon, \qquad \rho E = \rho\epsilon + \frac{\rho v_k^2}{2},$$

where $p$ is the pressure, $\rho$ is the density, $\vec{v} = (v_x, v_y, v_z)$ is the velocity vector, $\rho E$ is the total energy density, $\Phi$ is the gravitational potential of the gas itself, $\Phi_0$ is the contribution of the dark matter and stars to the gravitational potential, $\epsilon$ is the inner energy, and $q$ is the cooling function [48].

The collisionless component dynamics is described by the collisionless Boltzmann equation for the distribution function of particles $f(x, t, w)$ in the 6D position($x$) – velocity($w$) phase space:

$$\frac{\partial f}{\partial t} + w_k \frac{\partial f}{\partial x_k} + g_k \frac{\partial f}{\partial w_k} = 0.$$

The first moment of the collisionless Boltzmann equation are

$$n = \int mf \, dw, \qquad n\vec{u} = \int mfw \, dw,$$
$$\Pi_{ij} = \int mf(w_i - u_i)(w_j - u_j) \, dw = \Pi_{ji},$$
$$nE_{ij} = \Pi_{ij} + nu_i u_j,$$

where $\Pi_{ij}$ is the symmetric velocity dispersion tensor, $n$ is the density, $\vec{u} = (u_x, u_y, u_z)$ is the velocity vector, $nE_{ij}$ is the total energy density, $\Phi$ is the gravitational potential of the gas itself, $\Phi_0$ is the contribution of the dark matter and stars to the gravitational potential, $m$ is the particles mass.

We should use for the collisionless component a 3D model of the Boltzmann moment equations in the Cartesian coordinate system:

$$\frac{\partial n}{\partial t} + \frac{\partial n u_k}{\partial x_k} = 0,$$
$$\frac{\partial n u_i}{\partial t} + \frac{\partial n u_i u_k}{\partial x_k} = -\frac{\partial \Pi_{ik}}{\partial x_k} - n\frac{\partial(\Phi + \Phi_0)}{\partial x_i},$$
$$\frac{\partial n E_{ij}}{\partial t} + \frac{\partial n E_{ij} u_k}{\partial x_k} = -\frac{\partial(\Pi jk u_i + \Pi ik u_j)}{\partial x_k} - nu_i\frac{\partial(\Phi + \Phi_0)}{\partial x_j} - nu_j\frac{\partial(\Phi + \Phi_0)}{\partial x_i},$$
$$\frac{\partial \Pi_{ij}}{\partial t} + \frac{\partial \Pi_{ij} u_k}{\partial x_k} = -\Pi_{jk}\frac{\partial u_i}{\partial x_k} - \Pi_{ik}\frac{\partial u_j}{\partial x_k},$$
$$\Delta\Phi_0 = 4\pi n.$$

The main characteristic parameters are: $L = 10000$ parsec, $M_0 = 10^{11} M_\odot$, $G = 6.67 \cdot 10^{-11}$ N m$^2$/kg, $q = 2 \cdot 10^{-24}$ kg/s$^3$ m. Let us introduce a uniform grid in the 3D computation domain. The cells of the grid are: $x_i = ih_x$, $i = 1, \ldots, I_{\max}$, $y_k = kh_y$, $k = 1, \ldots, K_{\max}$, $z_l = lh_z$, $l = 1, \ldots, L_{\max}$, where $h_x$, $h_y$, $h_z$ are the mesh steps, $I_{\max}$, $K_{\max}$, $L_{\max}$ are the numbers of the mesh cells along the directions $x$, $y$, $z$: $h_x = x_{\max}/I_{\max}$, $h_y = y_{\max}/K_{\max}$, $h_z = z_{\max}/L_{\max}$. The solution of the gas dynamics equation is based on the Fluids-in-Cells and the Godunov method [39], which has shown a good advantage for astrophysical problems [2].

**2.1. Solving the gas dynamics equation.** The solution of the gas dynamics equations system is carried out in two stages. At the first (Eulerian) stage, the equations system describes a change in gas values as a result of pressure, gravity and cooling. The operator approach is used for the elimination of the mesh effect [49]. The values of the pressure $P$ and the velocity $V$ at all the cells boundaries are the exact solution to the linearized Eulerian stage equation system without potential and cooling function.

Let us consider 1D gas dynamics equations in the Cartesian coordinate system:

$$\frac{\partial \rho}{\partial t} + \left[v\frac{\partial \rho}{\partial x}\right] + \rho\frac{\partial v}{\partial x} = 0,$$
$$\frac{\partial v}{\partial t} + \left[v\frac{\partial v}{\partial x}\right] + \frac{1}{\rho}\frac{\partial p}{\partial x} = 0,$$
$$\frac{\partial p}{\partial t} + \left[v\frac{\partial p}{\partial x}\right] + \gamma p\frac{\partial v}{\partial x} = 0.$$

We can reject advective terms and consider 1D gas dynamics equations at the Eulerian stage:

$$\frac{\partial}{\partial t}\begin{pmatrix} \rho \\ v \\ p \end{pmatrix} + \begin{pmatrix} 0 & \rho & 0 \\ 0 & 0 & \rho^{-1} \\ 0 & \gamma p & 0 \end{pmatrix}\frac{\partial}{\partial x}\begin{pmatrix} \rho \\ v \\ p \end{pmatrix} = 0$$

The eigenvalues of this matrix are $\lambda_1 = 0$, $\lambda_2 = \sqrt{\frac{\gamma p}{\rho}}$, $\lambda_3 = -\sqrt{\frac{\gamma p}{\rho}}$. We could reject the first column and the first row and consider the equations

$$\frac{\partial q}{\partial t} + B\frac{\partial q}{\partial x} = 0,$$

where $q = (v, p)$, $B = R\Lambda L$, $R$ is the matrix of right eigenvectors, $L$ is the matrix of the left-hand side eigenvectors, $\Lambda$ is the diagonal matrix of eigenvalues, $RL = I$. Making the substitution $s = Lq$ we arrive to independent equations

$$\frac{\partial s}{\partial t} + \Lambda\frac{\partial s}{\partial x} = 0.$$

This system of equations has the exact solution at each of the cell boundaries, depending on the sign of the eigenvalues. Let us make the inverse substitution in $q = Rs$, and $q$ being the exact solution of equations at the Eulerian stage.

The eigenvalues and eigenvectors of 1D gas dynamics equations at the Eulerian stage are the following:

$$\lambda_1 = \sqrt{\frac{\gamma p}{\rho}}, \quad l_1 = \left(\frac{1}{\sqrt{\gamma p\rho}}, \frac{1}{\sqrt{\gamma p\rho}}\right), \qquad r_1 = \left(\frac{1}{\sqrt{\gamma p\rho}}, \frac{\rho\sqrt{\gamma p/\rho}}{\sqrt{\gamma p\rho}}\right);$$
$$\lambda_2 = -\sqrt{\frac{\gamma p}{\rho}}, \; l_2 = \left(\frac{\rho\sqrt{\gamma p/\rho}}{\sqrt{\gamma p\rho}}, -\frac{\rho\sqrt{\gamma p/\rho}}{\sqrt{\gamma p\rho}}\right), \; r_2 = \left(\frac{1}{\sqrt{\gamma p\rho}}, -\frac{\rho\sqrt{\gamma p/\rho}}{\sqrt{\gamma p\rho}}\right).$$

This system is linearly hyperbolic and has the following analytical solution

$$V = \frac{v_L + v_R}{2} + \frac{p_L - p_R}{2}\sqrt{\frac{\rho_L + \rho_R}{\rho_L\rho_R\gamma(p_L + p_R)}},$$
$$P = \frac{p_L + p_R}{2} + \frac{v_L - v_R}{2}\sqrt{\frac{\rho_L\rho_R\gamma(p_L + p_R)}{\rho_L + \rho_R}},$$

where $f_L$ and $f_R$ correspond to the values of a function at the left and right cells boundaries. These values are used in the Eulerian stage scheme.

At the second (Lagrangian) stage, the equations system contains divergent equations of the following form:

$$\frac{\partial f}{\partial t} + \mathrm{div}(f\vec{v}) = 0.$$

The Lagrangian stage describes the advective transportation process of all the gas quantities $f$. The initial version of the numerical method involved the computation of the contributions of the gas quantities to the adjacent cells [50]. The computation was based on the scheme velocity. However this approach is not suitable for computation accelerators (Nvidia Tesla or Intel

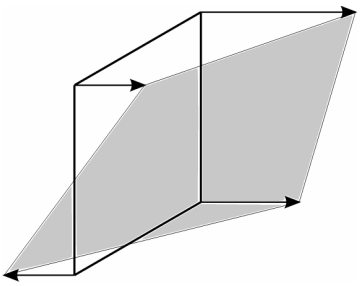

**Figure 1.** Stream gas dynamic quantities across the boundary defined by the rule of the total deformation of a cell

Xeon Phi, etc.). In order to show this, let us consider the solution of the above equation in the 1D form:

$$\frac{f_{ikl}^{n+1} - f_{ikl}^{n}}{\tau} + \frac{F_{i+1/2,kl}^{n+1/2} - F_{i-1/2,kl}^{n+1/2}}{h} = 0$$

where

$$F_{i+1/2,kl}^{n+1/2} = \frac{\sum v_{i+1/2,k\pm1,l\pm1} f_{ikl}^{+}}{4}$$

which is demonstrated by Figure 1.

**2.2. The method of solving the Boltzmann moment equations solution.** We can reject out advective terms for the 1D Boltzmann moment equations and consider six (instead of 10) equations of the system at the Eulerian stage:

$$\frac{\partial}{\partial t}\begin{pmatrix} u_x \\ u_y \\ u_z \\ \Pi_{xx} \\ \Pi_{xy} \\ \Pi_{xz} \end{pmatrix} + \begin{pmatrix} 0 & 0 & 0 & \rho^{-1} & 0 & 0 \\ 0 & 0 & 0 & 0 & \rho^{-1} & 0 \\ 0 & 0 & 0 & 0 & 0 & \rho^{-1} \\ 3\Pi_{xx} & 0 & 0 & 0 & 0 & 0 \\ 2\Pi_{xy} & \Pi_{xx} & 0 & 0 & 0 & 0 \\ 2\Pi_{xz} & 0 & \Pi_{xx} & 0 & 0 & 0 \end{pmatrix} \frac{\partial}{\partial x}\begin{pmatrix} u_x \\ u_y \\ u_z \\ \Pi_{xx} \\ \Pi_{xy} \\ \Pi_{xz} \end{pmatrix} = 0.$$

We repeat the approach described in the previous section. The eigenvalues and eigenvectors of the 1D Boltzmann moment equations at the Eulerian stage are

$$\lambda_1 = \sqrt{\frac{3\Pi_{xx}}{\rho}}, \qquad l_1 = \left(\frac{\rho\Pi_{xz}\sqrt{3}}{2\sqrt{\rho\Pi_{xx}}}, 0, 0, \frac{\Pi_{xz}}{2\Pi_{xx}}, 0, 0\right),$$

$$r_1 = \left(\frac{\sqrt{\Pi_{xx}}}{\Pi_{xz}\sqrt{3\rho}}, \frac{\Pi_{xy}\sqrt{3}}{\Pi_{xz}\sqrt{\rho\Pi_{xx}}}, \frac{1}{\sqrt{3\rho\Pi_{xx}}}, \frac{\Pi_{xx}}{\Pi_{xz}}, \frac{\Pi_{xy}}{\Pi_{xz}}, 1\right);$$

$$\lambda_2 = -\sqrt{\frac{3\Pi_{xx}}{\rho}}, \qquad l_2 = \left(-\frac{\rho\Pi_{xz}\sqrt{3}}{2\sqrt{\rho\Pi_{xx}}}, 0, 0, \frac{\Pi_{xz}}{2\Pi_{xx}}, 0, 0\right),$$

$$r_2 = \left(-\frac{\sqrt{\Pi_{xx}}}{\Pi_{xz}\sqrt{3\rho}}, -\frac{\Pi_{xy}\sqrt{3}}{\Pi_{xz}\sqrt{\rho\Pi_{xx}}}, -\frac{1}{\sqrt{3\rho\Pi_{xx}}}, \frac{\Pi_{xx}}{\Pi_{xz}}, \frac{\Pi_{xy}}{\Pi_{xz}}, 1\right);$$

$$\lambda_3 = \sqrt{\frac{\Pi_{xx}}{\rho}}, \qquad l_3 = \left(-\frac{\Pi_{xz}\sqrt{\rho}}{2\sqrt{\Pi_{xx}}}, 0, \frac{\sqrt{\rho\Pi_{xx}}}{2}, -\frac{\Pi_{xz}}{2\Pi_{xx}}, 0, \frac{1}{2}\right),$$

$$r_3 = \left(0, 0, \frac{1}{\sqrt{\rho\Pi_{xx}}}, 0, 0, 1\right);$$

$$\lambda_4 = \sqrt{\frac{\Pi_{xx}}{\rho}}, \qquad l_4 = \left(-\frac{\Pi_{xy}\sqrt{\rho}}{2\sqrt{\Pi xx}}, \frac{\sqrt{\rho\Pi_{xx}}}{2}, 0, -\frac{\Pi_{xy}}{2\Pi_{xx}}, \frac{1}{2}, 0\right),$$
$$r_4 = \left(0, \frac{1}{\sqrt{\rho\Pi_{xx}}}, 0, 0, 1, 0\right);$$
$$\lambda_5 = -\sqrt{\frac{\Pi_{xx}}{\rho}}, \qquad l_5 = \left(-\frac{\Pi_{xy}\sqrt{\rho}}{2\sqrt{\Pi_{xx}}}, -\frac{\sqrt{\rho\Pi_{xx}}}{2}, 0, -\frac{\Pi_{xy}}{2\Pi_{xx}}, \frac{1}{2}, 0\right),$$
$$r_5 = \left(0, -\frac{1}{\sqrt{\rho\Pi_{xx}}}, 0, 0, 1, 0\right);$$
$$\lambda_6 = -\sqrt{\frac{\Pi_{xx}}{\rho}}, \qquad l_6 = \left(\frac{\Pi_{xz}\sqrt{\rho}}{2\sqrt{\Pi_{xx}}}, 0, -\frac{\sqrt{\rho\Pi_{xx}}}{2}, -\frac{\Pi_{xz}}{2\Pi_{xx}}, 0, \frac{1}{2}\right),$$
$$r_6 = \left(0, 0, -\frac{1}{\sqrt{\rho\Pi_{xx}}}, 0, 0, 1\right).$$

This system is linearly hyperbolic and has the following analytical solution

$$u_x = \frac{u_x^L + u_x^R}{2} + \frac{\Pi_{xx}^L - \Pi_{xx}^R}{2}\left[\frac{1}{\sqrt{3\rho\Pi_{xx}}}\right],$$
$$u_y = \frac{u_y^L + u_y^R}{2} + \frac{\Pi_{xy}^L - \Pi_{xy}^R}{2}\left[\frac{1}{\sqrt{\rho\Pi_{xx}}}\right] + \frac{\Pi_{xx}^L - \Pi_{xx}^R}{2}\left[\frac{\Pi_{xy}(1-\sqrt{3})}{\Pi_{xx}\sqrt{3\rho\Pi_{xx}}}\right],$$
$$u_z = \frac{u_z^L + u_z^R}{2} + \frac{\Pi_{xz}^L - \Pi_{xz}^R}{2}\left[\frac{1}{\sqrt{\rho\Pi_{xx}}}\right] + \frac{\Pi_{xx}^L - \Pi_{xx}^R}{2}\left[\frac{\Pi_{xz}(1-\sqrt{3})}{\Pi_{xx}\sqrt{3\rho\Pi_{xx}}}\right],$$
$$\Pi_{xx} = \frac{\Pi_{xx}^L + \Pi_{xx}^R}{2} + \frac{u_x^L - u_x^R}{2}\left[\sqrt{3\rho\Pi_{xx}}\right],$$
$$\Pi_{xy} = \frac{\Pi_{xy}^L + \Pi_{xy}^R}{2} + \frac{u_y^L - u_y^R}{2}\left[\sqrt{\rho\Pi_{xx}}\right] + \frac{u_x^L - u_x^R}{2}\left[\frac{\Pi_{xy}\rho(\sqrt{3}-1)}{\sqrt{\rho\Pi_{xx}}}\right],$$
$$\Pi_{xz} = \frac{\Pi_{xz}^L + \Pi_{xz}^R}{2} + \frac{u_z^L - u_z^R}{2}\left[\sqrt{\rho\Pi_{xx}}\right] + \frac{u_x^L - u_x^R}{2}\left[\frac{\Pi_{xz}\rho(\sqrt{3}-1)}{\sqrt{\rho\Pi_{xx}}}\right],$$

where $f_L$ and $f_R$ correspond to the values of a function at the left and right cells boundaries. Parameters in square brackets should be averaged. These values are used in the Eulerian stage scheme for the Boltzmann moment equations.

**2.3. The Poisson equation solution** for the gravitational potential

$$\Delta(\Phi + \Phi_0) = 4\pi(\rho + n)$$

is based on 27 stencil points. The Fourier transform is used to solve the Poisson equation. The Poisson equation solution scheme in the Fourier space is

$$(\Phi + \Phi_0)_{jmn} = \frac{4\pi h^2(\rho + n)_{jmn}}{6(1 - (1 - \frac{2}{3}\sin^2(\frac{\pi j}{I}))(1 - \frac{2}{3}\sin^2(\frac{\pi m}{K}))(1 - \frac{2}{3}\sin^2(\frac{\pi n}{L})))}.$$

The Fast Fourier Transform is used for the direct and inverse transforms.

**2.4.** At each time step, checking for the correctness was used:

$$\kappa_{\text{gas}} = \int |\rho E - \rho\epsilon - \rho v^2/2|\, dx,$$
$$\kappa_{\text{bme}} = \int |nE_{ij} - \Pi_{ij} - nu_i u_j|\, dx.$$

The energy balance procedure at each time step is described in [51].

## 3. Parallel implementation

The necessity of three-dimensional simulation and the unsteady nature of the problem impose strict requirements for methods of solution. The recent rapid development of computer technologies has allowed carrying out intensive computations and obtaining physically correct results by means of the 3D codes. Using supercomputers makes possible to use large data volumes to improve the computation accuracy and, also, to accelerate computations. The main problem within the astrophysical code development is the efficient solution of gas dynamics equations and the Boltzmann moment equations since it takes up to 90 % of computation time (Figure 2).

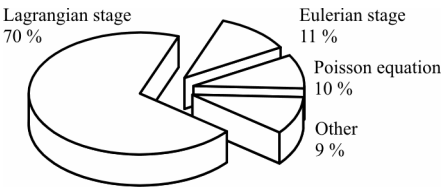


**Figure 2.** The portion of each stage in the total computation time

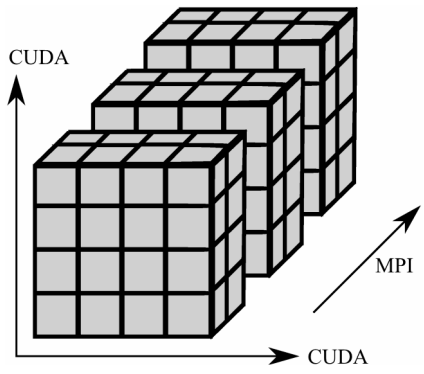


**Figure 3.** Domain decomposition for the solution of the hydrodynamic equations

The basis of the parallel implementation of a hydrodynamic solver is a three-dimensional domain decomposition. There is an MPI decomposition along the coordinate, while the other two coordinates the CUDA technology is used (Figure 3). The three-dimensional parallel Fast Fourier Transform is performed by the subroutine from the freeware FFTW library. In the future, such a Poisson solver will be ported to the GPU accelerators.

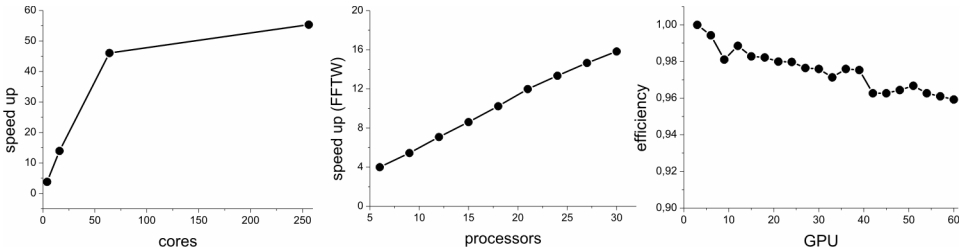


**Figure 4.** The speed up of gas dynamics equations and the Boltzmann moment equations on one GPU (left). The speed up of the Poisson equation solver, depending on the used cores (middle). Efficiency the parallel implementation of gas dynamics equations and the Boltzmann moment equations on the used GPU (right)

The parallel implementation is related to the topology and architecture of a hybrid supercomputer NKS-G6 of the Siberian Supercomputer Center ICMMG SB RAS. The modification of the numerical method for solving the hydrodynamic equations is implemented at every stage irrespective computation of the fluxes through each cell. In this case, the one-layer overlapping of the boundary points of the neighboring subdomains is needed. In the near future, such a modification of the method will be ported to Intel Xeon Phi accelerators.

In the case of a hybrid implementation, it is necessary to define two concepts of scalability:

- The strong scalability — the reduction of the computation time of one step of the same problem when a great number of devices is used.
- The weak scalability — saving the one step computation time and the same amount of tasks with increasing the number of devices at the same time.

The results of the program implementation efficiency are shown in Figure 4.

## 4. Testing the implementation

The GPUPEGAS code was verified on: 4 problems of a shock tube (3 of them were the Godunov tests for the gas dynamics equations and one test for the Boltzmann moment equations); a new Aksenov test; the Kelvin–Helmholtz and the Rayleigh–Taylor Instability tests; the author's cloud collision test, i.e., the collapse of rotating molecular cloud test.

**4.1. The Godunov tests** are based on the on a shock wave simulation. The table shows the initial configurations of the shock tube for the tests. The results of simulation are given in Figure 5.

**Table 1.** The initial state of the shock tube

| Test | $\rho_L$ | $v_L$ | $p_L$ | $\rho_R$ | $v_R$ | $p_R$ | $x_0$ | $t$ |
|---|---|---|---|---|---|---|---|---|
| 1 | 2 | 0 | 2 | 1 | 0 | 1 | 0.5 | 0.2 |
| 2 | 1 | −2 | 0.4 | 1 | 2 | 0.4 | 0.5 | 0.15 |
| 3 | 1 | 0 | 1000 | 1 | 0 | 0.01 | 0.5 | 0.012 |

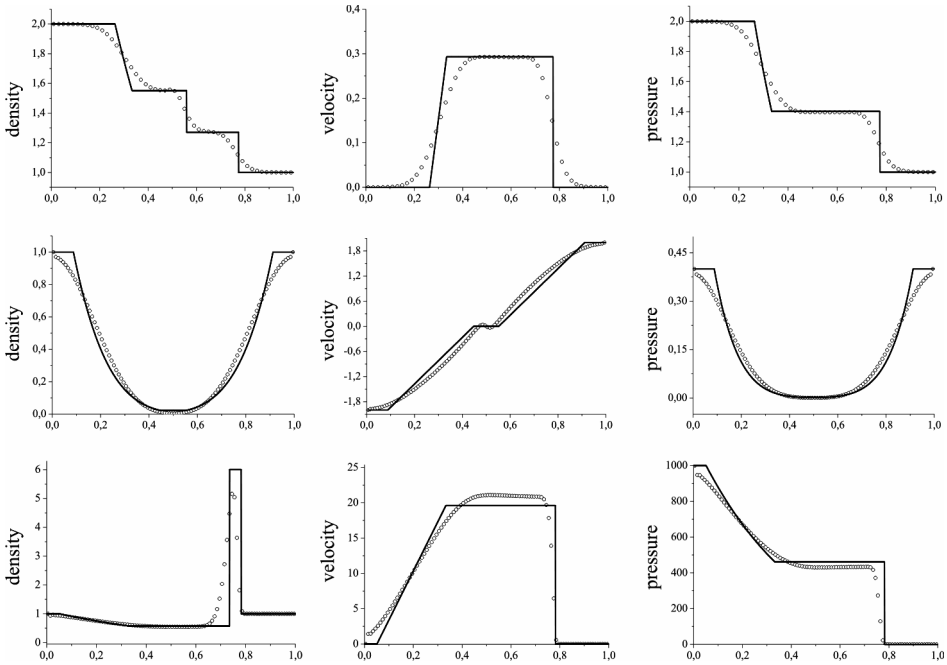


**Figure 5.** Distribution of density, velocity and pressure in the simulation of the first test (the top row), the second test (the middle row), and the third test (the bottom row). The solid line represents the exact solution, dots indicate the result of the computation. The purpose of the first test is to determine the correctness of the description of the contact discontinuity. In the second test, the gas with the same thermodynamic parameters expands, producing a rarefaction region in the center. The main objective of the third test is to check the stability of the numerical method

**4.2. The shock tube test for the Boltzmann moment equations.** The initial configurations of the Shock tube test for the Boltzmann moment equations are

$$[\rho, \Pi_{xx}, \Pi_{xy}, \Pi_{xz}, \Pi_{yy}, \Pi_{yz}, \Pi_{zz}, u_x, u_y, u_z] = \begin{cases} [2,2,1,1,1,1,1,0,0], & x \le 0.5, \\ [1,1,1,1,1,1,1,0,0], & x \le 0.5. \end{cases}$$

The results of simulation are given in Figure 6.

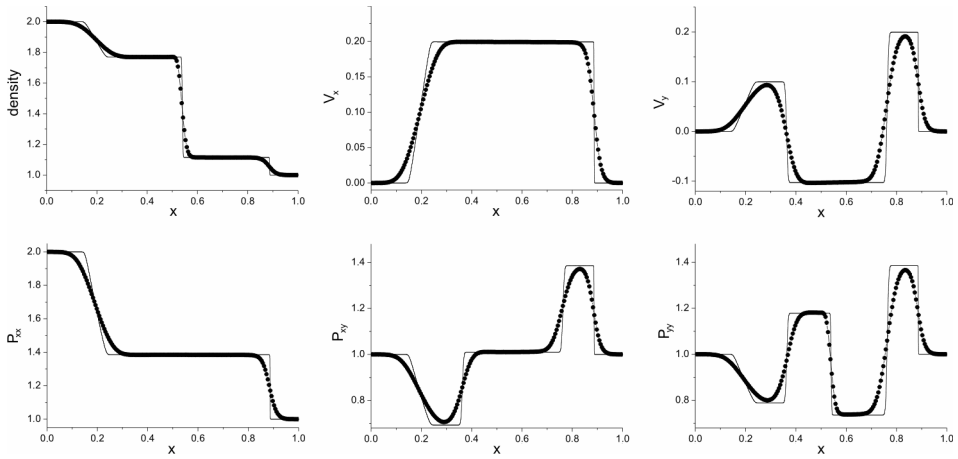


**Figure 6.** Distribution of density, velocity and the symmetric velocity dispersions tensor in the simulation of the shock tube test for the Boltzmann moment equations. The solid line represents the exact solution, dots indicate the result of the computation. The purpose of the test is to determine the correctness of the description of discontinuities

**4.3. The Aksenov test.** Consider the one-dimensional gas dynamics equations in the following form:

$$\frac{\partial u}{\partial t} + u\frac{\partial u}{\partial x} = -\frac{1}{\rho}\frac{\partial p}{\partial x}, \qquad \frac{\partial \rho}{\partial t} + \frac{\partial \rho u}{\partial x} = 0, \qquad \frac{p}{p_0} = \left(\frac{\rho}{\rho_0}\right)^{\gamma},$$

where $p$ is pressure, $\rho$ is density, $u$ is velocity, and $\gamma$ is the adiabatic index.

Let $l$ be a characteristic length, $\rho_0$ be the characteristic density, and $p_0$ be the characteristic pressure. Then the characteristic velocity is $u_0 = \sqrt{\gamma p_0/\rho_0}$ and the characteristic time is $t_0 = l/\sqrt{\gamma p_0/\rho_0}$. Select the dimensionless quantities $l = 1$, $p_0 = 1$, $\rho_0 = 1$, $\gamma = 3$ and $\lambda = 1/(\gamma - 1)$, $r = \rho^{1/2\lambda}$, $z = u/2\lambda$. Let us choose the initial data $r = 1 + 0.5\cos x$ and $z = 0$ [52]. Then the analytical solution on $[0, 2\pi]$ is

$$r(x,t) = 1 + 0.5\cos(x - zt)\cos(rt), \qquad z(x,t) = 0.5\sin(x - zt)\sin(rt).$$

The results of the simulation for the time $t = \pi/2$ are given in Figure 7.

Velocity is sufficiently well approximated by the numerical solution. The density has a jump in the center. This jump is of the same principle as temperature jump in the third Godunov test. Actually, we should have something of the type of a trace of entropy in this test, which is formed as a result of the "run-off" gas with zero velocity in this region. This feature focuses on a finite number of points and is reduced by splitting a mesh.

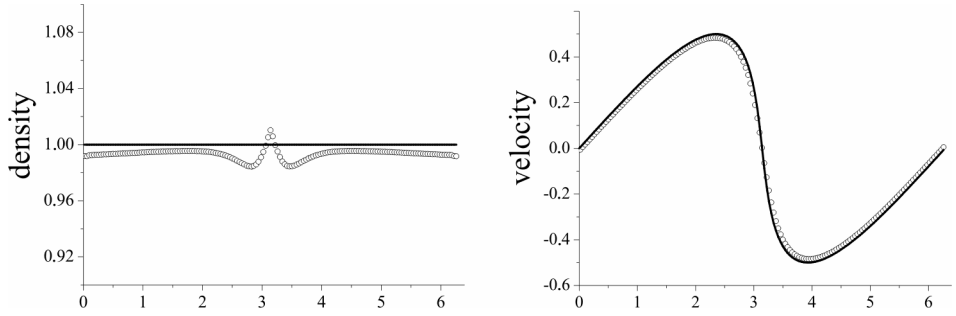


**Figure 7.** Distribution of density and velocity at the time $t = \pi/2$. The solid line shows the exact solution, points show computation

**4.4. The Kelvin–Helmholtz and the Rayleigh–Taylor instabilities.** The gravitational instability is the basis for the physical formulation of the problem resulting on a mathematical incorrectness. The numerical method used not suppress the physical instability. To check the correct reproduction of the instability, the code has been verified on the Rayleigh–Taylor and the Kelvin–Helmholtz instability. Rayleigh-Taylor instability verifies the playback capability of the gravitational term. The Kelvin–Helmholtz instability verifies the playback capability of the nonlinear hydrodynamic turbulence.

The initial data for the Rayleigh–Taylor instability — $[-0.5, 0.5]^2$ is the domain, $\gamma = 1.4$ is the adiabatic index,

$$\rho_0(x) = \begin{cases} 1, & r \le 0, \\ 2, & r > 0, \end{cases}$$

$p = 2.5 - \rho g y$ is the hydrostatic equilibrium pressure, $g$ is the free fall acceleration, $v_{y,0}(x, y) = A(y)[1 + \cos(2\pi x)][1 + \cos(2\pi y)]$, where

$$A(y) = \begin{cases} 10^{-2}, & |y| \le 0.01, \\ 0, & y > 0.01. \end{cases}$$

The initial data for the Kelvin–Helmholtz instability — $[-0.5, 0.5]^2$ is the domain, $\gamma = 1.4$,

$$\rho_0(x) = \begin{cases} 1, & r \le 0, \\ 2, & r > 0, \end{cases} \qquad v_x = \begin{cases} 0.5, & |y| \le 0.25, \\ -0.5, & |y| > 0.25, \end{cases}$$

$p = 2.5$, $v_{y,0}(x, y) = A(y)[1 + \cos(8\pi x)][1 + \cos(8\pi y)]$, where

$$A(y) = \begin{cases} 10^{-2}, & ||y| - 0.25| \le 0.01, \\ 0, & ||y| - 0.25| > 0.01. \end{cases}$$

The results of the Kelvin–Helmholtz and the Rayleigh–Taylor instability simulation are given in Figure 8.

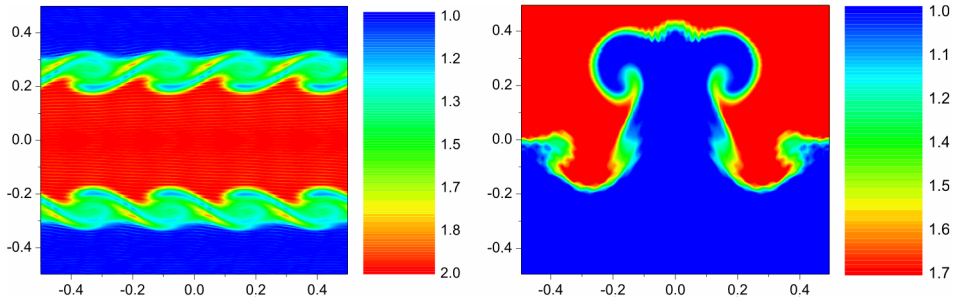


**Figure 8.** Density in Kelvin-Helmholtz (left) and Rayleigh-Taylor (right) Instability simulation.

**4.5. The author's cloud collision test.** Let us take a steady-state gas sphere in the situation of hydrostatic equilibrium as the initial state for the gas dynamics equations. The density distribution is obtained from the gas dynamics equation system together with the Poisson equation written down in the spherical coordinates:

$$\frac{\partial p}{\partial r} = -\frac{M(r)\rho}{r^2}, \quad \frac{\partial M}{\partial r} = 4\pi r^2 \rho, \quad p = (\gamma - 1)\rho\epsilon.$$

The density distribution is

$$\rho_0(r) = \begin{cases} 1 - r, & r \le 1, \\ 0, & r > 1. \end{cases}$$

Then the pressure and gravitational potential are the following:

$$p_0(r) = \begin{cases} -\dfrac{\pi r^2}{36}(9r^2 - 28r + 24) + \dfrac{5\pi}{36}, & r \le 1, \\ 0, & r > 1. \end{cases}$$

$$\Phi_0(r) = \begin{cases} -\dfrac{\pi}{3}(r^3 - 2r^2) - \dfrac{2\pi}{3}, & r \le 1, \\ -\dfrac{\pi}{3r}, & r > 1. \end{cases}$$

The initial distance between two gas clouds is 2.4, the collision velocity is 1. The results of simulation are given in Figure 9.

**4.6. The collapse of a rotation cloud.** For the research into the possibility of modeling the collapse of rotating molecular clouds we simulate a gas cloud bounded by the sphere with radius $R_0 = 100$ pc, the mass of the

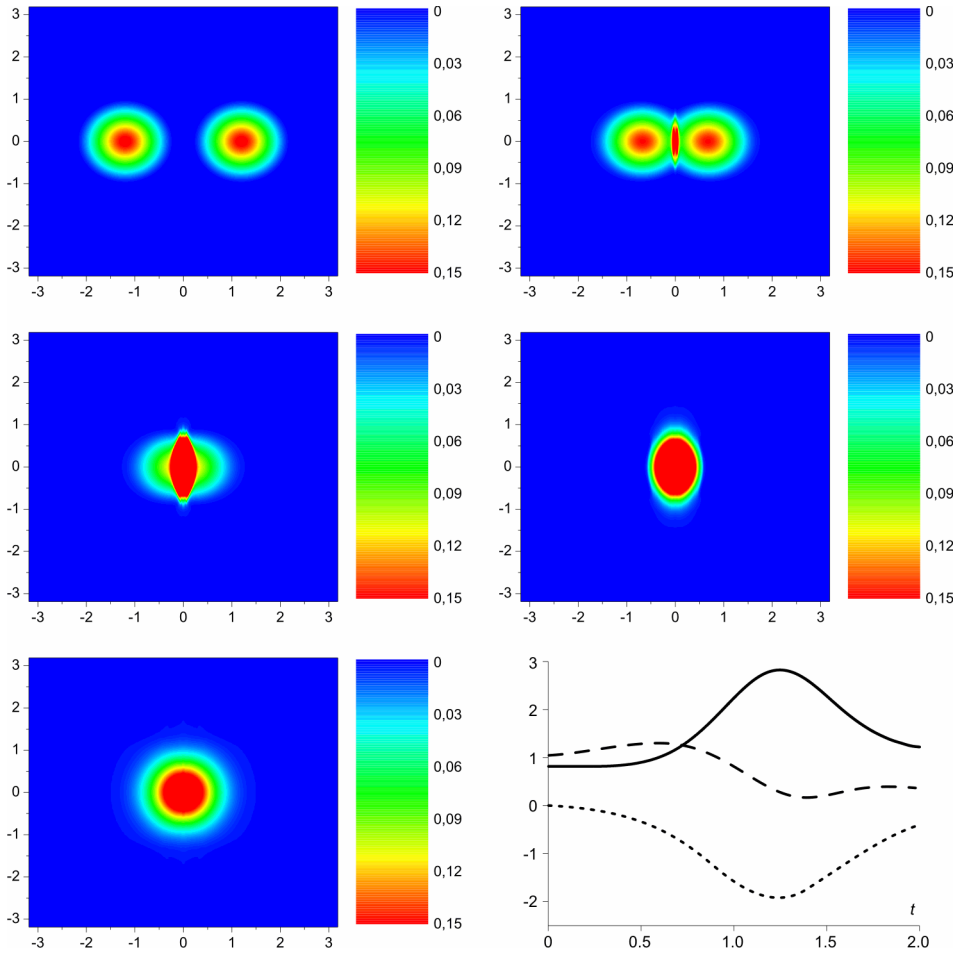


**Figure 9.** The author's cloud collision test. Dynamic of dimensionless density distribution is shown. The last figure shows the behavior of inner energy (solid line), kinetic energy (dashed line), and potential energy (dotted line). The mass of gas and total impulse are conserved. The conservation of energy was traced in the computation

cloud $M_g = 10^7 M_\odot$, the density $\rho(r) \simeq 1/r$, the temperature $T \approx 2000$ K, the angular velocity $\omega = 21$ km/s, the adiabatic index $\gamma = 5/3$, the sound speed $c \approx 3.8$ km/s. The main characteristic parameters are $L_0 = 100$ pc, $\rho_0 = 1.2 \cdot 10^{-18}$ kg/m$^3$, $v_0 = 21$ km/s. Then the dimensionless density $\rho = 1.0$, the pressure $p = 2 \cdot 10^{-2}$, the angular velocity $\omega = 1$, the adiabatic index $\gamma = 5/3$, the domain is $[0, 6.4]^3$. In this research, the behavior of energy has quantitatively coincidence (Figure 10) with the results by other authors [53].

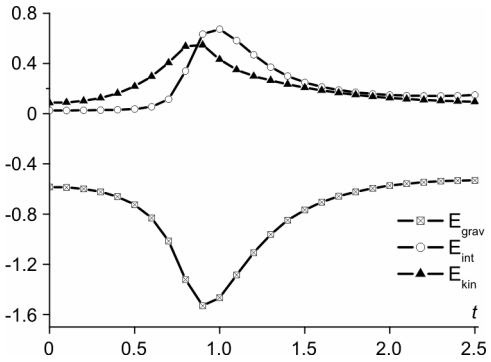


**Figure 10.** The behavior of energy in the collapse of molecular clouds simulation

## 5. Numerical simulation of galaxies collisions

The main objective of the code GPUPEGAS is modeling the galaxies collisions of different types and at different angles. As a model problem, we consider the collision of the disk galaxies at an angle. The first cloud is given as a spherical domain uniformly filled with gas $M_{\text{gas}} = 16 \cdot 10^{41}$ kg. The second cloud is given with respect to the ellipsoid axes $1 : 2 : 1$, inclined at 45 degrees to the axis of the collision. The clouds move in the opposite directions with the velocities $v_{\text{cr}} = 600$ km/s. Figure 11 shows the evolution of the collision and a "slim" splash of the interacting galaxies. The calculation was carried out using 96 GPU-accelerators cluster NKS-G6 of the Siberian Supercomputer Center ICM&MG SB RAS on the mesh $1024^3$ with $10^5$ time steps.

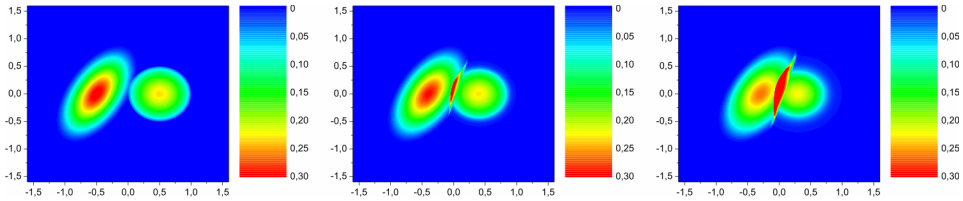

**Figure 11.** Dimensionless density of gas clouds at the initial time (left), at $1 \cdot 10^{14}$ s (middle), and at $2 \cdot 10^{14}$ s (right)

**5.1. The passage scenario of a central collision of two galaxies.** Let us show the possibility of scenarios of the galaxies passage in the two-phase model [39]. Two self-gravitating gas clouds are set in the 3D computational domain at the initial moment. Both clouds have the same distributions of gas parameters. Each cloud is a spherical domain uniformly filled with gas of the mass $M_{\text{gas}} = 16 \cdot 10^{41}$ kg and the stars and the dark matter with the mass $M_{\text{gas}} = 16 \cdot 10^{41}$ kg. The clouds move in the opposite directions with the velocities $v_{\text{cr}} = 800$ km/s. We should repeat the passage scenario of a

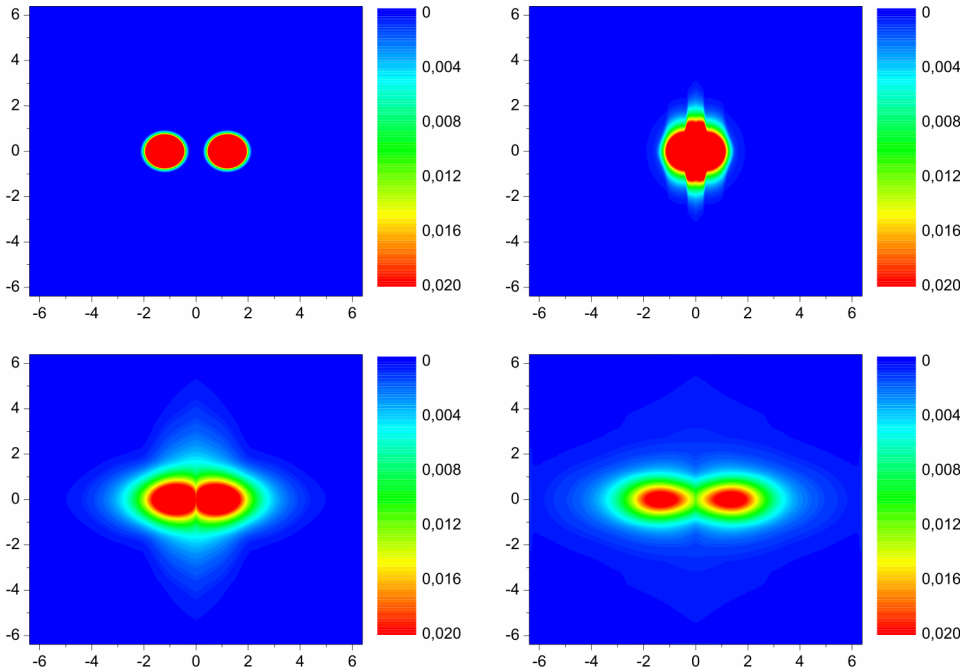


**Figure 12.** Dimensionless gas density in the collision plane, the scenario with the passage of galaxies: collision begins at the time $1 \cdot 10^{14}$ s (top left), the moment of collision at $10^{15}$ s (top right), the start of the passage of galaxies at $2.5 \cdot 10^{15}$ s (bottom left), and the end of the passage of galaxies at $4.6 \cdot 10^{15}$ s (bottom right)

central collision of two galaxies in the two-phase model. Figure 12 shows the evolution of the passage scenario of a central collision of two galaxies.

## 6. Conclusions and prospects for the future work

A new GPUPEGAS code for the simulation of interacting galaxies on a hybrid supercomputer by means of the GPU is described. The code is based on a combination of the Godunov method as well as on the original implementation of the FlIC method, specially adapted for the GPU-implementation. The Fast Fourier Transform is used for the Poisson equation solution in the GPUPEGAS. The software implementation of the above methods was tested on classical gas dynamics problems, a new Aksenov's test and classical gravitational gas dynamics problems. The Boltzmann moment equations approach was used for modeling stars and the dark matter. The possibility of scenarios of the galaxies passage in the two-phase model is shown. The scalability of the GPUPEGAS computational accelerators is shown. Maximum speed-up factors of 55 (as compared with 12.19 on GAMER code [35]) are demonstrated using one GPU. The maximum efficiency of 96 % (as compared

with 65 % in the GAMER code on 16 GPUs [35]) are demonstrated using 60 GPUs cluster NKS-G6 of the Siberian Supercomputer Center ICM&MG SB RAS.

## References

[1] Tutukov A., Fedorova A. The role of close passages of galaxies and the asymmetry of their dark haloes in the formation of their spiral patterns // Astronomy Reports. — 2006. — Vol. 50, Iss. 10. — P. 785–801.

[2] Tutukov A., Lazareva G., Kulikov I. Gas dynamics of a central collision of two Galaxies: merger, disruption, passage, and the formation of a new galaxy // Astronomy Reports. — 2011. — Vol. 55, Iss. 9. — P. 770–783.

[3] Gingold R.A., Monaghan J.J. Smoothed particle hydrodynamics: theory and application to non-spherical stars // Monthly Notices of the Royal Astronomical Society. — 1977. — Vol. 181. — P. 375–389.

[4] Luci L.B. A numerical approach to the testing of the fission hypothesis // The Astrophysical J. — 1977. — Vol. 82, No. 12. — P. 1013–1024.

[5] Collela P., Woodward P.R. The piecewise parabolic method (PPM) for gas-dynamical simulations // J. Comput. Phys. — 1984. — Vol. 54. — P. 174–201.

[6] Norman M. The impact of AMR in numerical astrophysics and cosmology // Lecture Notes in Computational Science and Engineering. — 2005. — Vol. 41. — P. 413–430.

[7] Hockney R.W., Eastwood J.W. Computer Simulation Using Particles. — New York: McGraw-Hill, 1981.

[8] Couchman H., Pearce F. Thomas P. Hydra Code Release. — http://arxiv.org/abs/astro-ph/9603116.

[9] Barnes J., Hut P. A hierarchical $O(N \log N)$ force-calculation algorithm // Nature. — 1986. — Vol. 324. — P. 446–449.

[10] Dubinski J., Kim J., Park C., Humble R. GOTPM: a parallel hybrid particle-mesh treecode // New Astronomy. — 2004. — Vol. 9. — P. 111–126.

[11] Fedorenko R. A relaxation method for solving elliptic difference equations // USSR Computational Mathematics and Mathematical Physics. — 1961. — Vol. 1. — P. 1092–1096.

[12] Godunov S.K. A difference scheme for numerical solution of discontinuous solution of hydrodynamic equations // Matematicheskii Sbornik. — 1959. — Vol. 47. — P. 271–306.

[13] Kulikovskii A.G., Pogorelov N., Semenov A. Mathematical Aspects of Numerical Solution of Hyperbolic Systems. — Moscow: Fizmatlit, 2001.

[14] Toro E.F. Riemann Solvers and Numerical Methods for Fluid Dynamics. — Heidelberg: Springer, 1999.

[15] Courant R., Isaacson E., Rees M. On the solution of nonlinear hyperbolic differential equations by finite difference // Communications on Pure and Applied Mathematics. — 1952. — Vol. 5, No. 3. — P. 243–255.

[16] Roe P. Approximate Riemann solvers, parameter vectors, and difference schemes // J. Comput. Phys. — 1997. — Vol. 135, Iss. 2. — P. 250–258.

[17] Engquist B., Osher S.J. One-sided difference approximations for nonlinear conservation laws // Mathematics of Computation. — 1981. — Vol. 36, No. 154. — P. 321–351.

[18] Harten A., Lax P.D., Van Leer B. On upstream differencing and Godunov-type schemes for hyperbolic conservation laws // SIAM Review. — 1983. — Vol. 25, No. 1. — P. 35–61.

[19] Einfeld B. On Godunov-type methods for gas dynamics // SIAM J. Numer. Anal. — 1988. — Vol. 25, No. 2. — P. 294–318.

[20] Batten P., Clarke N., Lambert C., Causon D.M. On the choice of save speeds for the HLLC Riemann solver // SIAM J. Comput. — 1997. — Vol. 18, No. 6. — P. 1553–1570.

[21] Van Leer B. Towards the ultimate conservative difference scheme. V - A second-order sequel to Godunov's method // J. Comput. Phys. — 1979. — Vol. 32. — P. 101–136.

[22] Pearce F., Couchman H. Hydra: a parallel adaptive grid code // New Astronomy. — 1997. — Vol. 2, Iss. 5. — P. 411–427.

[23] Wadsley J.W., Stadel J., Quinn T. Gasoline: a flexible, parallel implementation of TreeSPH // New Astronomy. — 2004. — Vol. 9, Iss. 2. — P. 137–158.

[24] Matthias S. GRAPESPH: cosmological smoothed particle hydrodynamics simulations with the special-purpose hardware GRAPE // Monthly Notices of the Royal Astronomical Society. — 1996. — Vol. 278, Iss. 4. — P. 1005–1017.

[25] Springel V. The cosmological simulation code GADGET-2 // Monthly Notices of the Royal Astronomical Society. — 2005. — Vol. 364, Iss. 4. — P. 1105–1134.

[26] Jin S., Xin Z. The relaxation schemes for systems of conservation laws in arbitrary space dimensions // Communications on Pure and Applied Mathematics. — 1995. — Vol. 48. — P. 235–276.

[27] Godunov S.K., Manuzina Yu.D., Nazareva M.A. Experimental analysis of convergence of the numerical solution to a generalized solution in fluid dynamics // Computational Mathematics and Mathematical Physics. — 2011. — Vol. 51. — P. 88–95.

[28] Ziegler U. Self-gravitational adaptive mesh magnetohydrodynamics with the NIRVANA coder // Astronomy and Astrophysics. — 2005. — Vol. 435. — P. 385–395.

[29] Mignone A., Plewa T., Bodo G. The piecewise parabolic method for multidimensional relativistic fluid dynamics // The Astrophysical J. — 2005. — Vol. 160. — P. 199–219.

[30] Hayes J. et al. Simulating radiating and magnetized flows in multiple dimensions with ZEUS-MP // The Astrophysical J. Supplement Series. — 2006. — Vol. 165. — P. 188–228.

[31] Teyssier R. Cosmological hydrodynamics with adaptive mesh refinement. A new high resolution code called RAMSES // Astronomy and Astrophysics. — 2002. — Vol. 385. — P. 337–364.

[32] Kravtsov A., Klypin A., Hoffman Y. Constrained simulations of the real universe. II. Observational signatures of intergalactic gas in the local supercluster region // The Astrophysical J. — 2002. — Vol. 571. — P. 563–575.

[33] Stone J., et al. Athena: a new code for astrophysical MHD // The Astrophysical J. Supplement Series. — 2008. — Vol. 178. — P. 137–177.

[34] Brandenburg A., Dobler W. Hydromagnetic turbulence in computer simulations // Computer Physics Communications. — 2002. — Vol. 147. — P. 471–475.

[35] Schive H., Tsai Y., Chiueh T. GAMER: a GPU-accelerated adaptive-mesh-refinement code for astrophysics // The Astrophysical J. — 2010. — Vol. 186. — P. 457–484.

[36] Murphy J., Burrows A. BETHE-hydro: an arbitrary Lagrangian–Eulerian multidimensional hydrodynamics code for astrophysical simulations // The Astrophysical J. Supplement Series. — 2008. — Vol. 179. — P. 209–241.

[37] Springel V. E Pur Si Muove: Galilean-invariant cosmological hydrodynamical simulations on a moving mesh // Monthly Notices of the Royal Astronomical Society. — 2010. — Vol. 401. — P. 791–851.

[38] Bruenn S. et al. 2D and 3D core-collapse supernovae simulation results obtained with the CHIMERA code // J. Physics. — 2009. — Vol. 180. — P. 1–5.

[39] Vshivkov V., Lazareva G., Snytnikov A., Kulikov I., Tutukov A. Hydrodynamical code for numerical simulation of the gas components of colliding galaxies // The Astrophysical J. Supplement Series. — 2011. — Vol. 194, Iss. 47. — P. 1–12.

[40] Gonzalez M., Audit E., Huynh P. HERACLES: a three-dimensional radiation hydrodynamics code // Astronomy and Astrophysics. — 2007. — Vol. 464. — P. 429–435.

[41] Krumholz M.R., Klein R.I., McKee C.F., Bolstad J. Radiation-hydrodynamic simulations of the formation of orion-like star clusters. I. Implications for the origin of the initial mass function // The Astrophysical J. — 2007. — Vol. 667, Iss. 74. — P. 1–16.

[42] Mignone A., et al. PLUTO: a numerical code for computational astrophysics // The Astrophysical J. Supplement Series. — 2007. — Vol. 170. — P. 228–242.

[43] Almgren A., et al. CASTRO: a new compressible astrophysical solver. I. Hydrodynamics and self-gravity // The Astrophysical J. — 2010. — Vol. 715. — P. 1221–1238.

[44] Feng Y., et al. Terapixel imaging of cosmological simulations // The Astrophysical J. Supplement Series. — 2011. — Vol. 197, Iss. 18. — P. 1–8.

[45] Ferrari A. et al. A new parallel SPH method for 3D free surface flows // High Performance Computing on Vector Systems 2009. — 2010. — Part 4. — P. 179–188.

[46] Van Straalen B., Shalf J., Ligocki T., Keen N., Yang W. Scalability challenges for massively parallel AMR applications // In IPDPS09: Proceedings of the 2009 IEEE International Symposium on Parallel and Distributed Processing, Washington, DC, USA. — P. 1–12.

[47] Mitchell N., Vorobyov E., Hensler G. Collisionless stellar hydrodynamics as an efficient alternative to N-body methods // Monthly Notices of the Royal Astronomical Society. — 2013. — Vol. 428. — P. 2674–2687.

[48] Sutherland R.S., Dopita M.A. Cooling functions for low-density astrophysical plasmas // The Astrophysical J. — 1993. — Vol. 88. — P. 253–327.

[49] Vshivkov V., Lazareva G., Kulikov I. An operator approach for numerical simulation of self-gravitation gasdynamic problem // Computational Technologies. — 2006. — Vol. 11, No. 3. — P. 27–35.

[50] Vshivkov V., Lazareva G., Kulikov I. A modified fluids-in-cell method for problems of gravitational gas dynamics // Optoelectronics, Instrumentation and Data Processing. — 2007. — Vol. 43, Iss. 6. — P. 530–537.

[51] Vshivkov V., Lazareva G., Snytnikov A., Kulikov I., Tutukov A. Computational methods for Ill-posed problems of gravitational gasodynamics // J. Inverse and Ill-posed Problems. — 2011. — Vol. 19, Iss. 1. — P. 151–166.

[52] Aksenov A.V. Symmetries and relations between solutions of a class of Euler–Poisson–Darboux equations // Reports of RAS. — 2001. — Vol. 381, Iss. 2. — P. 176–179.

[53] Petrov M.I., Berczik P.P. Simulation of the gravitational collapse and fragmentation of rotating molecular clouds // Astronomische Nachrichten. — 2005. — Vol. 326. — P. 505–513.